NASA/CR–20260003291

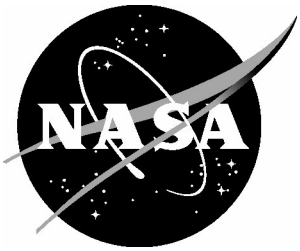

Optimization of a 10–Step Reduced CH_4/O_2 Combustion Mechanism for RDRE Applications

Shaye Yungster
HX5, LLC, Cleveland, OH

May 2026

NASA STI Program . . . in Profile

Since its founding, NASA has been dedicated to the advancement of aeronautics and space science. The NASA scientific and technical information (STI) program plays a key part in helping NASA maintain this important role.

The NASA STI program operates under the auspices of the Agency Chief Information Officer. It collects, organizes, provides for archiving, and disseminates NASA's STI. The NASA STI program provides access to the NTRS Registered and its public interface, the NASA Technical Reports Server, thus providing one of the largest collections of aeronautical and space science STI in the world. Results are published in both non-NASA channels and by NASA in the NASA STI Report Series, which includes the following report types:

- TECHNICAL PUBLICATION. Reports of completed research or a major significant phase of research that present the results of NASA Programs and include extensive data or theoretical analysis. Includes compilations of significant scientific and technical data and information deemed to be of continuing reference value. NASA counter-part of peer-reviewed formal professional papers but has less stringent limitations on manuscript length and extent of graphic presentations.

- TECHNICAL MEMORANDUM. Scientific and technical findings that are preliminary or of specialized interest, e.g., quick release reports, working papers, and bibliographies that contain minimal annotation. Does not contain extensive analysis.

- CONTRACTOR REPORT. Scientific and technical findings by NASA-sponsored contractors and grantees.

- CONFERENCE PUBLICATION. Collected papers from scientific and technical conferences, symposia, seminars, or other meetings sponsored or co-sponsored by NASA.

- SPECIAL PUBLICATION. Scientific, technical, or historical information from NASA programs, projects, and missions, often concerned with subjects having substantial public interest.

- TECHNICAL TRANSLATION. English-language translations of foreign scientific and technical material pertinent to NASA's mission.

Specialized services also include organizing and publishing research results, distributing specialized research announcements and feeds, providing information desk and personal search support, and enabling data exchange services.

For more information about the NASA STI program, see the following:

- Access the NASA STI program home page at http://www.sti.nasa.gov

NASA/CR–20260003291

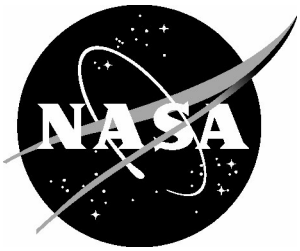

Optimization of a 10–Step Reduced CH_4/O_2 Combustion Mechanism for RDRE Applications

Shaye Yungster
HX5, LLC, Cleveland, OH

Prepared under Contract 80GRC020D0003

National Aeronautics and Space Administration

Glenn Research Center
Cleveland, Ohio 44135

May 2026

Available from:

NASA STI Program / Mail Stop 050
NASA Langley Research Center
Hampton, VA 23681-2199

Optimization of a 10–Step Reduced CH_4/O_2 Combustion Mechanism for RDRE Applications

Shaye Yungster
HX5, LLC, Cleveland, OH 44135, USA

Abstract

A 10-step, 9-species reduced mechanism for methane/oxygen combustion is evaluated and optimized for use in rotating detonation rocket engine (RDRE) simulations at an operating pressure of 10 bar. The mechanism is assessed against GRI-Mech 3.0 for ignition delay times, adiabatic equilibrium temperature and species, Chapman-Jouguet (CJ) detonation parameters, and laminar flame speed. A sequential Nelder–Mead optimization procedure is applied to the rate constants of reactions R1, R4, and R5, targeting ignition delay agreement over the equivalence ratio range φ = 1.0–1.4 and temperature range T = 1400–2000 K. The optimized mechanism achieves ignition delay agreement within 28% of GRI-Mech 3.0 for the temperature range relevant to RDRE operation (τ ≥ 5 μs). Adiabatic equilibrium temperatures and CJ detonation parameters are reproduced within 0.15% of GRI-Mech 3.0 values, confirming thermodynamic consistency of the mechanism. Laminar flame speed predictions deviate significantly from GRI-Mech 3.0, which is attributed to the absence of HO_2 chemistry in the reduced mechanism; this limitation does not affect RDRE simulation fidelity since laminar flame propagation is of secondary importance in RDREs.

Nomenclature

A	pre-exponential factor
a_i	concentration exponent for species i
D^c	Chapman-Jouguet detonation velocity, m/s
Ea	activation energy, cal/mol
k	rate constant
M^c	Chapman-Jouguet Mach number
n	temperature exponent
P	pressure, bar
P^c	Chapman-Jouguet pressure, bar
R	universal gas constant
Su	laminar flame speed, cm/s
SSR	sum of squared residuals (log-space)
T	temperature, K
T^c	Chapman-Jouguet temperature, K
τ	ignition delay time, μs
φ	equivalence ratio
ρ	density, kg/m³

I. Introduction

Rotating detonation rocket engines (RDREs) exploit the thermodynamic advantage of detonative combustion by sustaining one or more detonation waves that propagate continuously around an annular combustion chamber. Accurate numerical simulation of RDREs requires combustion mechanisms that are computationally efficient for three-dimensional unsteady flow solvers while still capturing the key chemical characteristics of the propellant mixture, particularly ignition delay and energy release behavior.

Many RDRE concepts currently under investigation employ methane–oxygen propellants due to their relevance to modern launch systems and in-space propulsion architectures. Although several detailed methane combustion mechanisms exist (e.g., Refs. 1,2), they typically contain a large number of species and reactions, making them computationally expensive for large-scale three-dimensional simulations. Furthermore, many of these mechanisms were developed for conventional combustion environments and are not specifically optimized for the high-pressure, high-temperature, and

highly transient conditions encountered in RDRE operation. Consequently, there is a need for reduced methane–oxygen combustion mechanisms tailored to RDRE applications.

This report presents a new reduced methane–oxygen combustion mechanism consisting of 10 reactions and 9 species that is specifically developed for RDRE simulations. The performance of the mechanism is evaluated by comparison with GRI-Mech 3.0 in terms of ignition delay, equilibrium composition, Chapman–Jouguet (CJ) detonation properties, and laminar flame speed. Mechanism development is based on an optimization procedure applied to three key rate constants over an RDRE-relevant equivalence ratio range at a nominal combustor pressure of 10 bar.

Development of the reduced mechanism began with construction of a baseline model derived from an existing 10-step ethylene combustion mechanism developed by Singh and Jachimowsky[3]. In this baseline formulation, the ethylene fuel decomposition reaction was replaced with a methane fuel decomposition reaction while retaining the remaining nine reactions unchanged. The rate constants for the methane breakup reaction were then adjusted using a trial-and-error procedure to match ignition delay times predicted by a more detailed methane–oxygen mechanism consisting of 133 reactions and 39 species that is provided in the LSENS code[4]. This calibration was performed at an equivalence ratio of $\varphi = 1.0$ and a pressure of 10 bar. The resulting model is referred to in this report as the baseline 10-step mechanism.

After establishing the baseline mechanism, a systematic optimization procedure was implemented to improve agreement with detailed-mechanism predictions over a broader range of equivalence ratios relevant to RDRE operation.

This report presents:

1. An evaluation of the baseline 10-step mechanism against GRI-Mech 3.0 for ignition delay, equilibrium composition, CJ detonation properties, and laminar flame speed.
2. A sequential optimization of three key reaction rate constants to improve ignition delay predictions across the RDRE-relevant equivalence ratio range.
3. An assessment of the performance of the optimized reduced mechanism.

II. Mechanism Description

2.1. The Baseline 10-Step Mechanism

The baseline reduced mechanism consists of 10 reversible elementary reactions among 9 species: CH_4, O_2, CO, H_2, CO_2, OH, H, O, and H_2O. The reaction set and corresponding Arrhenius rate parameters are listed in Table 1. Reaction Rate constants follow the modified Arrhenius expression

$$k = AT^n \exp\left(-\frac{E_a}{RT}\right)$$

Transport properties for all species are computed using Lennard–Jones parameters adopted from GRI-Mech 3.0 to ensure consistency with the reference mechanism used in this study.

Table 1. Baseline 10-step CH_4/O_2 mechanism.

Rxn	Reaction	A (cm-mol-s)	n	Ea (cal/mol)	Notes
R1	$2\ CH_4 + O_2 \rightleftharpoons 2\ CO + 4\ H_2$	2.00×10^{19}	0.0	52,000	Fuel breakup
R2	$CO + O + M \rightleftharpoons CO_2 + M$	5.30×10^{13}	0.0	-4540.0	efficiencies: {H2: 2.5, H2O: 16.0}
R3	$CO + OH \rightleftharpoons CO_2 + H$	4.40×10^{6}	1.5	-740.0	CO oxidation
R4	$H_2 + O_2 \rightleftharpoons OH + OH$	1.70×10^{13}	0.0	48000.0	Chain init.
R5	$H + O_2 \rightleftharpoons OH + O$	2.60×10^{14}	0.0	16800.0	Chain branch.
R6	$H_2 + OH \rightleftharpoons H_2O + H$	2.20×10^{13}	0.0	5150.0	
R7	$O + H_2 \rightleftharpoons OH + H$	1.80×10^{10}	1.0	8900.0	
R8	$OH + OH \rightleftharpoons H_2O + O$	6.30×10^{13}	0.0	1090.0	
R9	$H + H + M \rightleftharpoons H_2 + M$	6.40×10^{17}	-1.0	0.0	efficiencies: {H2: 2.5, H2O: 16.0}
R10	$OH + H + M \rightleftharpoons H_2O + M$	2.20×10^{22}	-2.0	0.0	efficiencies: {H2: 2.5, H2O: 16.0}

2.2. Reference Mechanism

GRI-Mech 3.0 (Ref. 5) is used as the reference detailed chemical kinetic mechanism for all comparisons presented in this report. The mechanism contains 325 elementary reactions among 53 species and has been extensively validated for methane combustion across a broad range of temperatures, pressures, and equivalence ratios.

In this work, GRI-Mech 3.0 serves as the benchmark against which the performance of the reduced 10-step mechanism is evaluated, including comparisons of ignition delay, equilibrium composition, Chapman–Jouguet detonation properties, and laminar flame speed.

III. Computational Methods

3.1. Simulation Platform

All calculations were performed using Cantera 3.1.0 (Ref. 6). Ignition delay and equilibrium calculations were carried out using a constant-pressure adiabatic reactor. Chapman–Jouguet detonation parameters were obtained using a direct thermodynamic solver, and laminar flame speeds were computed using a freely propagating, one-dimensional adiabatic flame model with mixture-averaged transport properties.

Nominal conditions used for ignition delay evaluation were a pressure of P = 10 bar, an equivalence ratio range of φ = 1.0–1.4, and an initial temperature range of T = 1400–2000 K.

3.2. Ignition Delay Definition

The ignition delay time, τ, is defined as the time required for the temperature in a constant-pressure adiabatic reactor to increase by 10% above its initial value. This definition provides a robust and consistent indicator of ignition for reduced mechanisms and corresponds closely to the onset of the primary heat release region.

Each reactor simulation is initialized with the unburned methane–oxygen mixture at the specified temperature, pressure, and equivalence ratio. The system is integrated in time until either the temperature rise exceeds 400 K or a maximum simulation time of 5 ms is reached.

3.3. Chapman-Jouguet Detonation Solver

CJ detonation parameters are computed using a thermodynamic equilibrium approach consistent with the methodology employed in the NASA Chemical Equilibrium with Applications (CEA) code[7]. For a trial detonation velocity D, the post-shock state is determined using the Rankine–Hugoniot jump relations together with the CJ sonic condition.

The shocked mixture is then equilibrated at constant enthalpy and pressure (HP equilibrium). The detonation velocity is iteratively adjusted using Brent's root-finding method until the Mach number of the combustion products satisfies the sonic CJ condition. This procedure yields the thermodynamic CJ state without explicitly resolving the internal detonation reaction-zone structure.

3.4. Optimization Method

The mechanism optimization targets agreement with GRI-Mech 3.0 ignition delay predictions over the parameter space: φ =1.0–1.4, T=1400–2000 K, P=10 bar.

Data points where the GRI-Mech ignition delay satisfies $\tau_{GRI} < 5$ μs are excluded from the objective function, since these extremely short timescales are not critical to RDRE simulations.

The objective function is a uniform-weight log-space sum of squared residuals:

$$SSR = \sum [\ln(\frac{\tau_{trial}}{\tau_{GRI}})]^2$$

where the summation extends over all active (T, φ) grid points. The log-space formulation ensures that multiplicative errors are treated consistently; for example, a factor-of-two error at 1 μs is penalized equally to a factor-of-two error at 100 μs.

The free parameters in the optimization are the Arrhenius coefficients (*A, n, Ea*) for three reactions:

- R1: ($2\ CH_4 + O_2 \rightleftharpoons 2\ CO + 4\ H_2$)
- R4: ($H_2 + O_2 \rightleftharpoons OH + OH$)
- R5: ($H + O_2 \rightleftharpoons OH + O$)

This yields a total of nine adjustable parameters. All reactions are treated as reversible, with reverse rate constants computed from equilibrium constants derived from thermodynamic data, thereby enforcing detailed balance.

The Optimization proceeds sequentially: R5 is optimized first (most sensitive to ignition delay timing), followed by R4,

then R1. After the sequential adjustments, a final joint optimization of all nine parameters is performed.

All the parameter optimization is performed using the Nelder–Mead simplex method[8], a derivative-free numerical optimization algorithm that is widely used for problems where the objective function is nonlinear, noisy, or expensive to evaluate. In the present work, each evaluation of the objective function requires multiple reactor simulations, making gradient-based methods difficult to apply. The Nelder–Mead method is well suited to this type of problem because it requires only function evaluations and does not rely on derivatives of the objective function.

In an optimization problem with N adjustable parameters, the Nelder–Mead method operates on a geometric object called a simplex, which consists of N+1 points in parameter space. Each point corresponds to a specific set of trial parameter values. For example, when optimizing the three Arrhenius coefficients (A,n,Ea) of a single reaction, the simplex consists of four points representing four different candidate parameter sets.

At each iteration, the algorithm evaluates the objective function at all simplex points and identifies the best and worst-performing parameter sets. The simplex is then systematically modified to explore improved regions of the parameter space. This modification is achieved through a sequence of geometric operations applied to the worst point in the simplex:

- Reflection: The worst point is reflected across the centroid of the remaining points in an attempt to move toward a better region of parameter space.
- Expansion: If the reflected point significantly improves the objective function, the algorithm expands further in that direction to accelerate progress.
- Contraction: If reflection does not produce improvement, the simplex contracts toward the best point, reducing the search region.
- Shrink: If contraction also fails, the entire simplex is shrunk toward the best point, allowing the algorithm to refocus around a promising region.

Through repeated application of these operations, the simplex progressively moves toward a set of parameters that minimizes the objective function. The method is particularly useful for moderate-dimensional problems such as the present case with nine adjustable parameters.

The geometric operations used by the Nelder–Mead algorithm are illustrated schematically in Fig. 1. For clarity, the example shown is for a two-parameter optimization problem, where the simplex becomes a triangle.

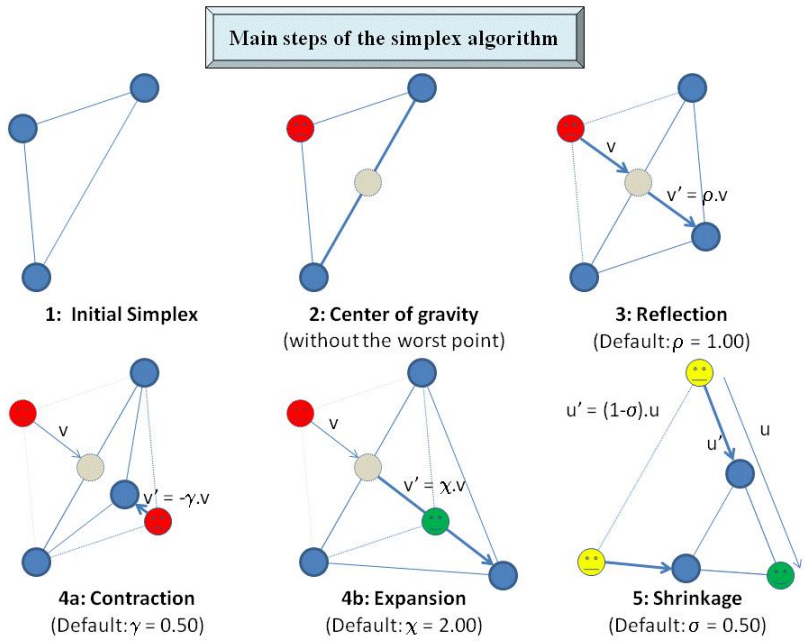

Figure 1: Illustration of the Nelder–Mead simplex optimization method in a two-parameter space. The simplex consists of three points (a triangle) representing candidate parameter sets. At each iteration the objective function is evaluated at the simplex vertices and the worst point is replaced through geometric transformations. The algorithm first attempts a reflection step to move away from the worst point. If improvement continues, an expansion step explores further in that direction. If reflection fails to improve the objective function, a contraction step moves the simplex toward the best point. If contraction also fails, the simplex undergoes a shrink operation in which all vertices move toward the current best point. Repeated application of these operations drives the simplex toward the parameter set that minimizes the objective function.

The Nelder–Mead algorithm is implemented in this work using the scipy.optimize.minimize function from the SciPy scientific computing library for Python. SciPy is an open-source numerical library that provides tools for optimization, integration, linear algebra, and scientific computing.

The scipy.optimize.minimize routine is a general-purpose interface for numerical optimization. It allows the user to specify:

- The objective function to be minimized (in this case the ignition-delay error metric),
- The initial guess for the parameters,
- The optimization algorithm (Nelder–Mead in this study), and
- Various stopping criteria and algorithm settings.

For the Nelder–Mead method, minimize evolves the simplex automatically from an explicit initial simplex that was constructed around the baseline parameter set.

Each call to the objective function triggers a full set of ignition delay simulations over the 3φ×7*T* grid. The optimization therefore proceeds iteratively, with the simplex gradually adjusting the Arrhenius parameters until improvements in the objective function become negligible or the specified evaluation limit is reached.

IV. Results

4.1. Optimized Rate Parameters

The optimized Arrhenius parameters for reactions R1, R4, and R5 are compared with their original values in Table 2. Optimization reduced the weighted sum of squared residuals (SSR) from 1.65 for the baseline mechanism to 0.40 for the optimized mechanism, corresponding to a 76% reduction in log-space ignition delay error across the optimization grid.

This improvement demonstrates the effectiveness of the optimization method, and that modest adjustments to a small number of kinetically important reactions can significantly improve ignition delay predictions while preserving the compact structure of the reduced mechanism.

Table 2. Comparison of baseline and optimized Arrhenius rate parameters.

Rxn	Parameter	Baseline	Optimized	Change
R1	*A*	2.00×10^{19}	4.01×10^{22}	+2000×
R1	*n*	0.0	−0.351	—
R1	*Ea*	52,000	68,057	+31%
R4	*A*	1.70×10^{13}	1.09×10^{12}	−94%
R4	*n*	0.0	−0.031	—
R4	*Ea*	48,000	49,665	+3.5%
R5	*A*	2.60×10^{14}	6.34×10^{14}	+144%
R5	*n*	0.0	+0.335	—
R5	*Ea*	16,800	14,179	−16%

4.2. Ignition Delay

Ignition delay times computed with the baseline and optimized 10-step mechanism are compared to GRI-Mech 3.0 in Tables 3–6 and Figure 2. Results are shown for φ = 1.0, 1.2, and 1.4 at P = 10 bar in Figs. 2a-2c. Data points marked with an asterisk correspond to conditions where $\tau_{GRI} < 5$ μs; these points were excluded from the optimization objective because such extremely short ignition times are not relevant to RDRE simulation.

The optimized mechanism shows a significant improvement in ignition delay prediction, particularly for φ = 1.2, where the errors decrease significantly across the active temperature range. (maximum error of 12%) The optimized mechanism more accurately reproduces the shape of the GRI-Mech curve than the baseline mechanism. At φ = 1.0 the optimized mechanism slightly overpredicts ignition delay by up to 28%, while at φ = 1.4 it underpredicts ignition delay by up to 27%. This systematic trend reflects a limitation of the 10-step mechanism in reproducing the detailed equivalence-ratio sensitivity of methane ignition. Because the reduced mechanism employs globalized reaction pathways, it cannot match the φ-dependence predicted by the detailed mechanism across the full stoichiometric-to-rich range.

The optimized mechanism was also evaluated at φ = 2.0. This equivalence ratio was not included in the optimization, and therefore is a true out-of-sample test. It shows how well the optimized R1/R4/R5 parameters generalize beyond the training range. Fig. 2d, shows that the optimized mechanism maintains a reasonable ignition delay accuracy (errors up to 52%), maintains the correct curve shape and slightly reduces the ignition delay under-prediction at low temperatures.

Table 3. Ignition delay comparison at φ = 1.0, P = 10 bar.

T (K)	τ_GRI (μs)	τ_base (μs)	τ_opt (μs)	err_base (%)	err_opt (%)
1400	96.65	68.79	111.82	−28.8	+15.7
1500	36.76	32.65	40.29	−11.2	+9.6
1600	15.75	17.49	17.21	+11.1	+9.3
1700	7.50	10.30	8.38	+37.3	+11.7
1800*	3.91	6.56	4.53	+67.7	+15.7
1900*	2.20	4.45	2.66	+102.6	+21.4
2000*	1.31	3.18	1.69	+142.4	+28.6

Table 4. Ignition delay comparison at φ = 1.2, P = 10 bar.

T (K)	τ_GRI (μs)	τ_base (μs)	τ_opt (μs)	err_base (%)	err_opt (%)
1400	108.09	60.85	98.83	−43.7	−8.6
1500	40.59	28.92	35.70	−28.7	−12.0
1600	17.10	15.51	15.28	−9.3	−10.6
1700	7.99	9.14	7.45	+14.4	−6.8
1800*	4.09	5.82	4.03	+42.1	−1.7
1900*	2.27	3.95	2.37	+74.2	+4.7
2000*	1.34	2.83	1.50	+110.6	+12.1

Table 5. Ignition delay comparison at φ = 1.4, P = 10 bar.

T (K)	τ_GRI (μs)	τ_base (μs)	τ_opt (μs)	err_base (%)	err_opt (%)
1400	120.30	55.67	90.35	−53.7	−24.9
1500	44.73	26.48	32.70	−40.8	−26.9
1600	18.58	14.21	14.01	−23.5	−24.6
1700	8.54	8.38	6.83	−1.9	−20.0
1800*	4.31	5.33	3.70	+23.9	−14.2
1900*	2.35	3.62	2.18	+53.8	−7.3
2000*	1.38	2.59	1.38	+87.8	+0.2

Table 6. Ignition delay comparison at φ = 2.0, P = 10 bar. [Out-of-sample]

T (K)	τ_GRI (μs)	τ_base (μs)	τ_opt (μs)	err_base (%)	err_opt (%)
1400	160.80	47.73	77.35	−70.3	−51.9
1500	58.64	22.73	28.06	−61.2	−52.2
1600	23.64	12.21	12.05	−48.4	−49.0
1700	10.47	7.20	5.89	−31.2	−43.7
1800	5.07	4.59	3.19	−9.5	−37.1
1900*	2.68	3.12	1.89	+16.3	−29.6
2000*	1.53	2.24	1.20	+45.8	−21.8

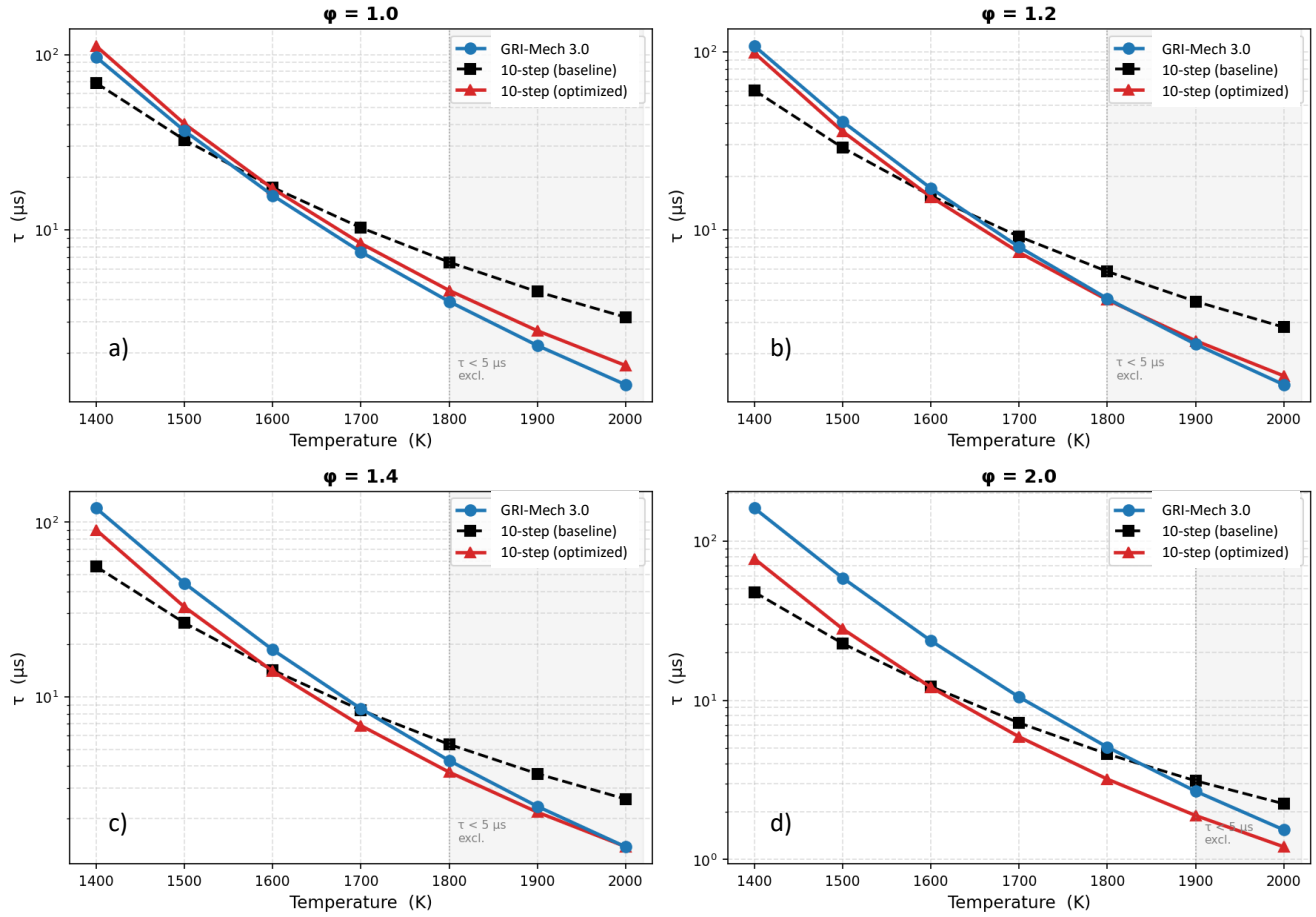

Figure 2: Ignition delay vs.T for φ = 1.0–2.0 at P = 10 bar. Blue circles: GRI-Mech 3.0; black squares: 10-step baseline; red triangles: 10-step optimized. Shaded region indicates τ < 5 μs (excluded from optimization).]

Figure 3 presents temperature–time profiles for the three combustion mechanisms under two representative conditions: (a) φ = 1.0 with an initial temperature of 1700 K, and (b) φ = 1.2 with an initial temperature of 1500 K. The results show that the optimized mechanism closely reproduces the shape of the GRI-Mech curve. This agreement is significant because the curve shape reflects the rate of heat release, which is a critical factor in modeling detonative combustion.

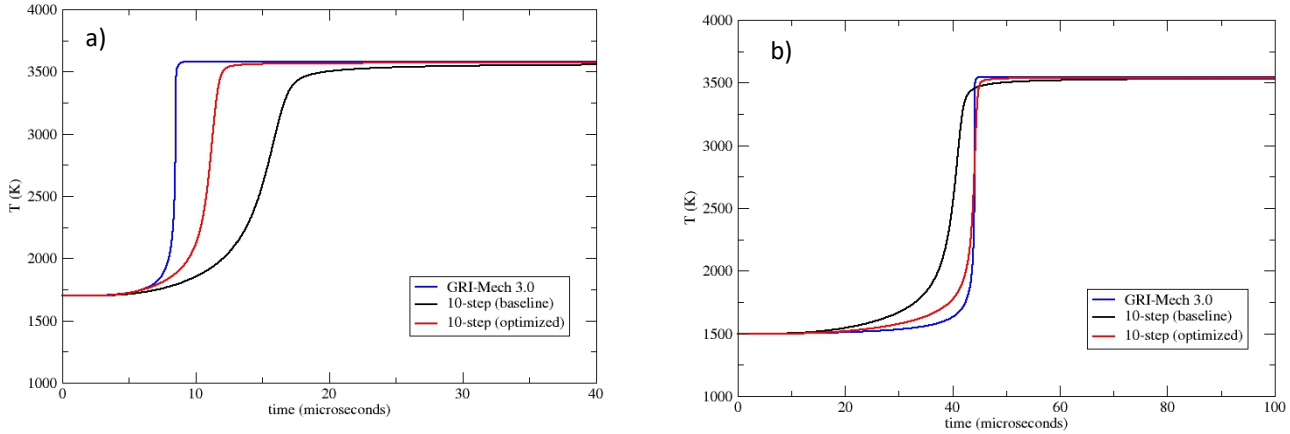

Figure 3: Temperature–time profiles for a) φ = 1.0; T_{init} = 1700 K and b) φ = 1.2; T_{init} = 1500 K, at P = 10 bar for the three combustion mechanisms.

4.3. Adiabatic Equilibrium

Adiabatic equilibrium temperatures and major species mole fractions were computed using constant-enthalpy, constant-pressure (HP) equilibrium calculations for both mechanisms at φ = 1.0, P = 10 bar, and initial temperatures T = 1400–2000 K. The resulting equilibrium temperatures and some of the species mole fractions are summarized in Table 7.

The equilibrium temperatures predicted by the two mechanisms agree to within 0.15% across all initial conditions, confirming that the thermodynamic data in the 10-step mechanism are consistent with GRI-Mech 3.0, and that enough species are included to properly account for dissociation phenomena. Similarly, the predicted equilibrium species concentrations closely match those from GRI-Mech 3.0, with the largest deviation observed for OH at approximately 5%. This agreement is expected since the equilibrium state is determined solely by the thermodynamic properties of the species and is independent of kinetic rate parameters.

Table 7. Adiabatic equilibrium temperature and species mole fraction comparison at φ = 1.0, P = 10

T_init (K)	T_eq 10-step	T_eq GRI-3.0	CO2 10-step	CO2 GRI-3.0	H2O 10-step	H2O GRI-3.0	OH 10-step	OH GRI-3.0	H 10-step	H GRI-3.0
1400	3519.4	3524.8	0.0920	0.0920	0.3537	0.3562	0.1238	0.1171	0.0547	0.0555
1500	3547.2	3552.6	0.0889	0.0889	0.3463	0.3489	0.1260	0.1192	0.0574	0.0582
1600	3572.1	3577.5	0.0858	0.0859	0.3390	0.3415	0.1282	0.1213	0.0602	0.0610
1700	3594.3	3599.7	0.0828	0.0829	0.3315	0.3341	0.1303	0.1234	0.0631	0.0639
1800	3614.2	3619.6	0.0799	0.0800	0.3241	0.3267	0.1323	0.1253	0.0661	0.0669
1900	3619.3	3624.7	0.0771	0.0772	0.3166	0.3193	0.1343	0.1272	0.0692	0.0700
2000	3624.3	3629.2	0.0743	0.0744	0.3092	0.3119	0.1363	0.1291	0.0724	0.0732

4.4. Chapman-Jouguet Detonation Parameters

CJ detonation parameters were computed at P = 10 bar, T = 300 K, φ = 1.0 for both mechanisms. The results are presented in Table 8.

All computed CJ parameters agree to within 0.15%, demonstrating excellent agreement between the reduced and detailed mechanisms. In particular, the predicted CJ detonation velocity and Mach number are identical to within numerical precision, confirming that the 10-step mechanism accurately reproduces the thermodynamic energy release of the methane–oxygen system.

As with equilibrium calculations, CJ detonation parameters depend only on the equation of state and thermodynamic properties of the reactants and equilibrium products. Consequently, the agreement observed here is largely independent of the kinetic parameter optimization.

Table 8. Chapman-Jouguet detonation parameters at φ = 1.0, P = 10 bar, T = 300 K.

Parameter	10-step mech.	GRI-Mech 3.0	Difference (%)
D^{c-} (m/s)	2490.76	2490.73	0.00
P^{c-}/P_0	30.553	30.576	−0.08
T^{c-}/T_0	13.862	13.881	−0.14
ρ^{c-}/ρ_0	1.803	1.804	−0.06
M^{c-}	6.989	6.989	0.00
T^{c-} (K)	4158.5	4164.2	−0.14
P^{c-} (bar)	309.58	309.81	−0.08

4.5. Laminar Flame Speed

Laminar flame speeds were computed using Cantera's freely-propagating 1D adiabatic flame solver with mixture-averaged transport at an unburned temperature T = 300 K. Calculations were performed over the equivalence ratio range φ

= 0.8–1.6 at P = 10 bar. Results are presented in Fig. 4.

Both the baseline and optimized 10-step mechanisms significantly under-predict laminar flame speed relative to GRI-Mech 3.0. This discrepancy is expected for a highly reduced mechanism. Laminar flame propagation in methane–oxygen mixtures is strongly dominated by diffusive transport of radicals, particularly those related to H_2 chemistry. The 10-step mechanism collapses all hydrogen chemistry into just H, OH, O, H_2, and H_2O with only a handful of reactions. It is missing the full H_2/O_2 sub-mechanism (HO_2, H_2O_2 and their reactions) that GRI-Mech has, which are important carriers of the chain-branching reactions that drives flame propagation. Without those pathways the flame simply cannot propagate at the correct speed.

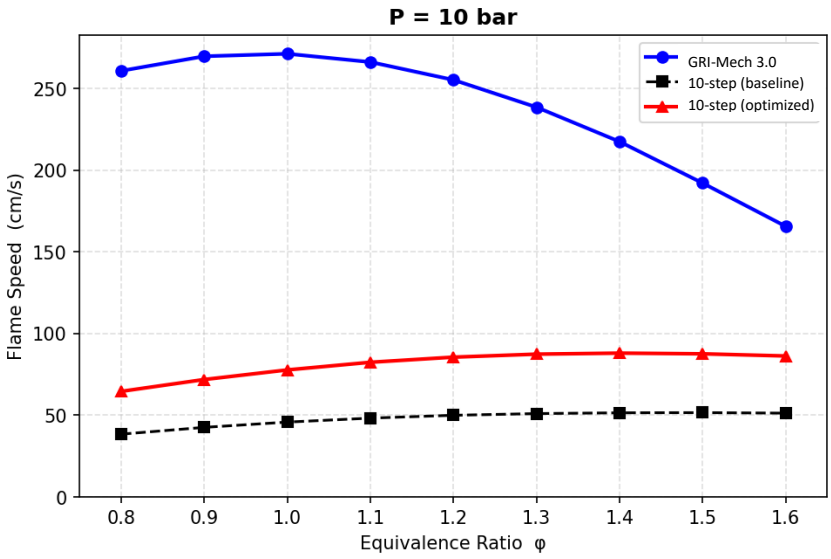

Figure 4: Laminar flame speed vs. equivalence ratio for CH_4/O_2 at T=300K and P=10 bar.

This limitation is not critical for RDRE applications because combustion occurs mainly in the detonation regime. Residence times of the unburned mixture in the chamber are extremely short, typically less than one millisecond. Over such short timescales, a laminar flame propagating at a characteristic speed of only a few meters per second would advance only a very small distance before being overtaken by the rotating detonation wave. Consequently, laminar, diffusion-controlled flame propagation contributes negligibly to the overall combustion process.

For RDRE simulations, the most relevant validation metrics are therefore ignition delay time—which determines how rapidly the mixture begins to react—and Chapman–Jouguet detonation properties, which determine heat release, detonation wave speed and thermodynamic state. The optimized mechanism reproduces both of these quantities with good accuracy. It should be noted, however, that parasitic (deflagrative) combustion is often observed in RDREs; however, the mechanisms governing its onset, its interaction with the detonation wave, and its overall impact on engine performance remain incompletely understood and are the subject of ongoing research.

V. Summary and Conclusions

The 10-step reduced CH_4/O_2 mechanism was evaluated and optimized for RDRE simulation conditions at P = 10 bar. The following conclusions are drawn:

- The 10-step mechanism reproduces CJ detonation parameters within 0.15% of GRI-Mech 3.0 and adiabatic equilibrium temperatures within 0.15%, confirming thermodynamic consistency.
- Ignition delay errors of the 10-step baseline mechanism are significant, particularly at rich conditions ($\varphi > 1.2$), with the baseline mechanism under-predicting ignition delay by up to 70% at $\varphi = 2.0$.
- Sequential Nelder-Mead optimization of the Arrhenius parameters for reactions R1, R4, and R5 reduces the weighted log-space SSR by 76% (from 1.65 to 0.40) over the φ = 1.0–1.4 range.
- The optimized 10-step mechanism achieves excellent agreement with GRI-Mech 3.0 at $\varphi = 1.2$ (errors < 12%) and acceptable agreement at φ = 1.0 and 1.4 (errors < 28%) for T = 1400–1700 K. At higher temperatures, the absolute differences are on the order of 1 microsecond, which are of negligible importance in RDRE simulations.
- Laminar flame speeds are significantly under-predicted, in part due to the absence of HO_2 chemistry, which plays an important role in radical transport and flame propagation.

Future work should consider extending the mechanism to include HO_2 chemistry, specifically the reactions

- H+O2 +M⇌HO2 +M
- HO2 +H⇌OH+OH

The first reaction becomes increasingly important at high pressures. Inclusion of these reactions may also improve both high-pressure ignition delay predictions and the equivalence-ratio dependence of ignition delay while maintaining a relatively compact reduced mechanism.

The optimization methodology developed in this study can be utilized to optimize the CH_4/O_2 mechanism at different operating conditions, or applied to the development of reduced combustion mechanisms involving other fuel/oxidizer combinations.

Acknowledgments

This study was supported by NASA under contract number 80GRC020D0003. Claude (Anthropic) was utilized as an AI assistant providing support with Python scripting for mechanism evaluation and optimization.

References

[1] Yungster, S., and Rabinowitz, M. J., "Computation of Shock-Induced Combustion Using a Detailed Methane-Air Mechanism," Journal of Propulsion and Power, Vol. 10, No. 5, 1994, pp. 609–617.

[2] Petersen, E.L. and Hanson, R.K., "Reduced Kinetics Mechanisms for Ram Accelerator Combustion," Journal of Propulsion and Power, Vol. 15, No. 4, 1999, pp. 591–600.

[3] Singh, D.J. and Jachimowski, C.J., "Quasiglobal Reaction Model for Ethylene Combustion," AIAA Journal, Vol. 32, No 1, pp 213-216 (1994)

[4] Radhakrishnan, K., "LSENS: Multipurpose Kinetic and Sensitivity Analysis Code for Homogeneous Gas-Phase reactions," AIAA Journal, Vol. 41, 845-855 (2003).

[5] Smith, G. P., Golden, D. M., Frenklach, M., Moriarty, N. W., Eiteneer, B., Goldenberg, M., Bowman, C. T., Hanson, R. K., Song, S., Gardiner, W. C., Lissianski, V. V., and Qin, Z., "GRI-Mech 3.0," http://www.me.berkeley.edu/gri_mech/, 2000.

[6] Cantera Development Team, "Cantera: An Object-Oriented Software Toolkit for Chemical Kinetics, Thermodynamics, and Transport Processes," Version 3.1.0, 2024. https://doi.org/10.5281/zenodo.8137090.

[7] Gordon, S. and McBride, B., "Computer program for calculation of complex chemical equilibrium compositions and applications. I Analysis," NASA RP-1311, (1994).

[8] Nelder, J. A., and Mead, R., "A Simplex Method for Function Minimization," The Computer Journal, Vol. 7, No. 4, 1965, pp. 308–313.